

Tri-Buffer Process: A New Approach to Obtain High-Quality ZnO Epitaxial Films on Sapphire Substrates

Z.X. MEI,^{1,4} X.L. DU,¹ Y. WANG,¹ M.J. YING,¹ Z.Q. ZENG,¹ H.T. YUAN,¹
J.F. JIA,² Q.K. XUE,^{1,2} and Z. ZHANG³

1.—Beijing National Laboratory for Condensed Matter Physics, Institute of Physics, Chinese Academy of Sciences, Beijing, 100080, China. 2.—Department of Physics, Tsinghua University, Beijing, 100084, China. 3.—Beijing University of Technology, Beijing, 100022, China. 4.—E-mail: zxmei@aphy.iphy.ac.cn

A tri-buffer method was applied to achieve layer-by-layer growth of high-quality ZnO films on sapphire (0001) substrates by rf plasma-assisted molecular beam epitaxy (MBE). After sufficient nitridation of the substrate, MgO and ZnO buffer layers were subsequently deposited on the resulting AlN layer. An atomically smooth ZnO surface with a roughness less than 1 nm in a $10\ \mu\text{m} \times 10\ \mu\text{m}$ scanned area was obtained with this method. The crystal quality was also improved, as characterized by reflection high-energy electron diffraction (RHEED), x-ray diffraction (XRD), Raman spectroscopy, and transmission electron microscopy (TEM). The results indicate that the tri-buffer process could reduce the large lattice mismatch between ZnO and nitrided sapphire and facilitate the two-dimensional (2-D) growth of the ZnO epilayer. A model is proposed to understand the observations.

Key words: ZnO, MgO, sapphire, tri-buffer, molecular beam epitaxy (MBE)

During the last decade, developments in the field of ZnO-based wide band gap materials have been striking. Currently, high-quality epitaxial layers can be grown by various methods, and efforts can be made on the fabrication of related optoelectronic devices.^{1–11} By far, most studies have been focused on ZnO-on-sapphire heteroepitaxy^{6,7} due to the high crystal quality, low cost, and hexagonal surface structure of sapphire substrates. However, the large lattice mismatch (18.3%) and thermal expansion mismatch (–13.2 and –64.5% perpendicular and parallel to the *c* direction, respectively) between ZnO and *c*-plane sapphire make the high-quality film growth difficult and complex. Some buffer techniques have been developed to solve this problem. Deposition of a low-temperature (LT) ZnO nucleation layer has been widely used prior to high-temperature (HT) epilayer,¹² and high-quality ZnO growth on MgO-buffered sapphire substrate has been thoroughly studied and optimized.^{13–15} Pre-growth nitridation was employed in our previous experiments to modify the sapphire surface.^{16,17}

This two-buffer method was found to be able to achieve the growth of unipolar and single-domain ZnO films. In those works, however, we found that the AlN layer formed by sapphire nitridation is not relaxed. Hence, the mismatch between ZnO and AlN is still as large as 18.3%, which makes further improvements in crystal quality impossible. In this paper, we report our approach to this issue by applying a tri-buffer process, that is, inserting a thin MgO layer between the ZnO and AlN layers. It was found that MgO can reduce the large lattice mismatch and facilitate the nucleation. An atomically smooth ZnO epilayer with improved quality was obtained, as confirmed by reflection high-energy electron diffraction (RHEED), x-ray diffraction (XRD), Raman spectroscopy, transmission electron microscopy (TEM), and atomic force microscopy (AFM).

The ZnO samples were prepared on sapphire (0001) substrates using an rf plasma-assisted molecular beam epitaxy (MBE) system. The base pressure in the growth chamber was $\sim 1 \times 10^{-10}$ Torr. The substrates were preconditioned by oxygen plasma at 180°C and then exposed to nitrogen radicals for 1 h with an rf power of 450 W and a nitrogen flux of 3 standard cubic centimeters per

minute (scm). After nitridation, a thin MgO layer was deposited at 450°C, followed by thermal annealing at 750°C for 20 min. When the temperature ramped down to 450°C, the growth of LT-ZnO buffer was turned on, followed by annealing at 780°C in oxygen plasma ambient. After these buffer growth steps, HT epilayer growth started at 650°C. For a better understanding of the mechanism governing the MgO buffer effects, the ZnO epilayer on the nitrated sapphire substrate without the MgO buffer layer was also grown under the same growth conditions. The evolution of the entire growth was monitored in situ by RHEED, and XRD, Raman, and AFM measurements were performed to characterize the crystallinity and surface morphology. The interface microstructures were studied by high-resolution TEM (HRTEM).

The growth of ZnO epilayers on nitrated sapphire with and without MgO buffer was first investigated by RHEED. Figures 1a and b show the RHEED patterns recorded from the sapphire surface before

and after nitridation, respectively. An unrelaxed thin AlN layer forms with a 30° in-plane rotation with respect to the substrate after nitridation. Detailed information can be found in our previous paper.^{16,17}

On the nitrated sapphire substrate, MgO patterns overlap on AlN patterns (MgO[111]//AlN[111], MgO[11 $\bar{2}$]//AlN[11 $\bar{2}$]). This follows a typical Stranski–Krastanov growth mode, that is, an initial two-dimensional (2-D) wetting layer and a subsequent three-dimensional (3-D) island growth (not shown here). The transition from 2-D to 3-D is very fast, only tens of seconds (the corresponding thickness is about 1 nm¹⁴). After that, the spotty patterns were maintained even after HT annealing (Fig. 1c). The 3-D growth is caused by the lattice mismatch (7.8%) between MgO (111) and unrelaxed AlN (111), which demonstrates that the compressive strains are partly released by the formation of islands. This facilitates the coalescence of the subsequent ZnO layer, which will be discussed later.

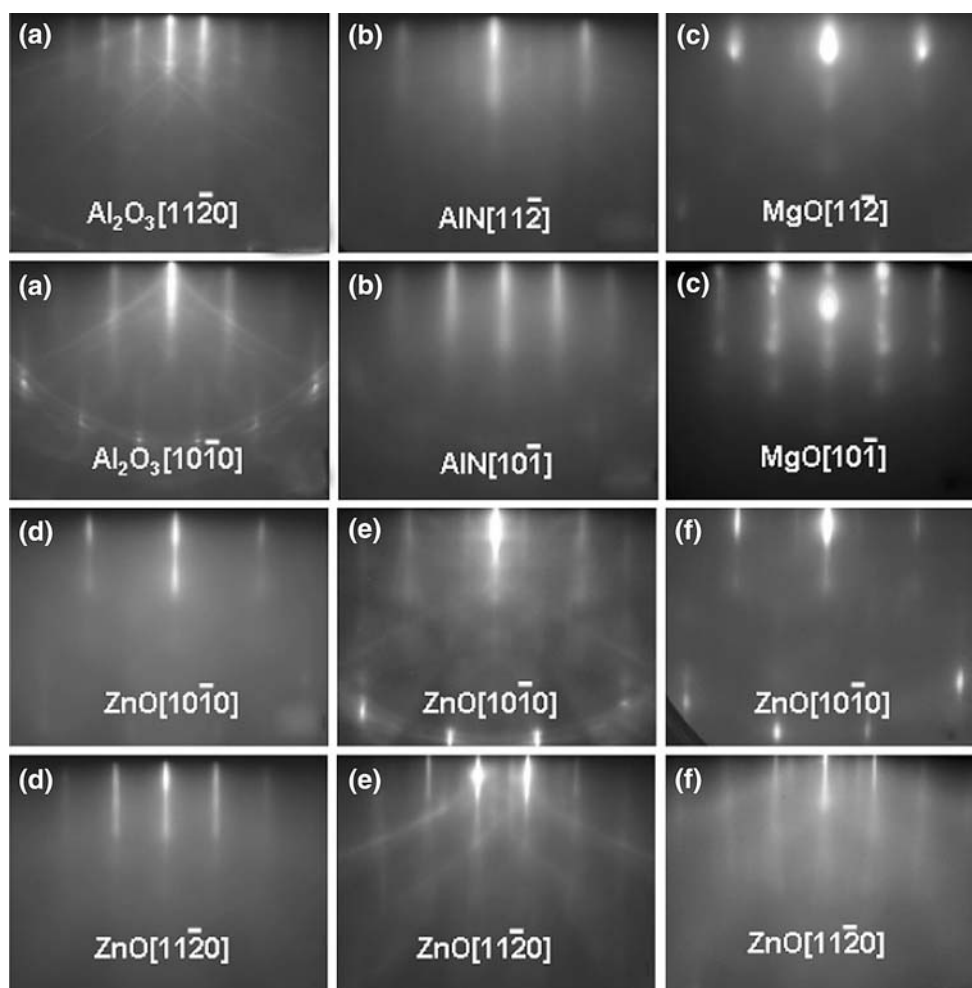


Fig. 1. RHEED patterns along the $[10\bar{1}0]$ and $[11\bar{2}0]$ e-beam azimuths observed during growth: (a) before sapphire nitridation, (b) after sapphire nitridation, (c) MgO buffer layer after annealing, (d) ZnO buffer layer after annealing with MgO buffer layer, (e) as-grown ZnO epilayer with MgO buffer layer, and (f) annealed ZnO epilayer without MgO buffer layer.

When the growth of ZnO is turned on, spotty patterns of ZnO appear superimposing on MgO's patterns with a rod space 9% smaller (not shown here). As the growth goes on, the RHEED spots became gradually elongated and remain until the end of the ZnO buffer layer growth. After annealing, sharp streaky RHEED patterns (Fig. 1d) can be observed, indicating the achievement of a flat ZnO surface.

The growth of the ZnO epilayer then starts at 650°C. After a few minutes, a strong specular spot appears and a 3×3 reconstruction is observed, which were maintained until the end of growth, as shown in Fig. 1e. It should be noticed that the appearance of well-defined Kikuchi lines offers convincing evidence of the high crystal quality and smooth surface.

In the case of the ZnO epilayer on nitrided sapphire substrate without MgO buffer layer, the diffuse streaky AlN patterns disappeared right after the beginning of ZnO buffer growth. The appearance of spotty ZnO patterns takes a much longer time than that using the MgO insertion layer, which is attributed to the larger lattice mismatch and worse wetting property. No reconstruction patterns were observed during the epilayer growth. After annealing, the RHEED patterns became streaky with a 3×3 reconstruction (Fig. 1f), but Kikuchi lines were not observed, which indicates an inferior crystal quality and a relatively rough surface.

The difference in surface morphology of the samples was further revealed by AFM images (Fig. 2a and b). As shown in the figures, a rough surface with an island structure was observed without the use of MgO buffer (Fig. 2a), while an extremely smooth surface was obtained after using MgO buffer (Fig. 2b). The root-mean-square values of the surface roughness are about 20 nm and less than 1 nm for a $10 \mu\text{m} \times 10 \mu\text{m}$ scan area, respectively. The observation of steps and terraces in Fig. 2b indicates a layer-by-layer growth of the ZnO epilayer. This 2-D growth presents an obvious contrast to the

3-D growth of the ZnO overlayer directly grown on the nitrided sapphire substrate (Fig. 2a), which was definitely promoted by the use of MgO buffer.

Here, it can be clearly seen that the insertion of the thin MgO layer plays a key role in obtaining a smooth surface. First, MgO reduces the large lattice mismatch between the ZnO and nitrided sapphire from 18.3% to 9% between ZnO and MgO, partly relaxes the misfit strain through formation of islands, and effectively decreases the defect density in the epilayer. These MgO islands also serve as nucleation sites, increase the wetting of a ZnO overlayer, and facilitate its 2-D growth, which was proved by the streaky RHEED patterns of the ZnO layer. Hence, this MgO layer is very helpful for improving the quality and surface morphology of the ZnO epilayer. On the other hand, 3-D growth predominates over 2-D growth in the case of the two-buffer process due to the large lattice mismatch between ZnO and unrelaxed AlN. The misfit dislocation was found at the interface between the ZnO and unrelaxed AlN layer,¹⁶ and the existence of a higher defect density results in an inferior crystal quality and rough surface morphology.

The role of the MgO buffer layer was further assessed by XRD measurements. The full-width at half-maximum of the skew symmetric $(10\bar{1}2)$ ω -scan of the ZnO epilayer was decreased from 1332 arcsec to 720 arcsec, which indicates the decrease of the twist component in the epilayer and the achievement of a better crystalline quality. Similarly, the narrower characteristic ZnO E_2 (high) peak (437.0 cm^{-1}) in the Raman spectra also verified the quality improvement after inserting a LT-MgO layer, compared to the one without the MgO layer (7.7 cm^{-1} cf. 17.4 cm^{-1} , or 9.6 meV cf. 21.6 meV).

A cross-sectional HRTEM study was carried out to determine the interface microstructure between the MgO buffer layer, the nitrided layer, and the sapphire substrate. These images were recorded near the $[10\bar{1}0]_{\text{sapph}}$ zone axis. In Fig. 3a, the HRTEM image shows the cross section of the ZnO/

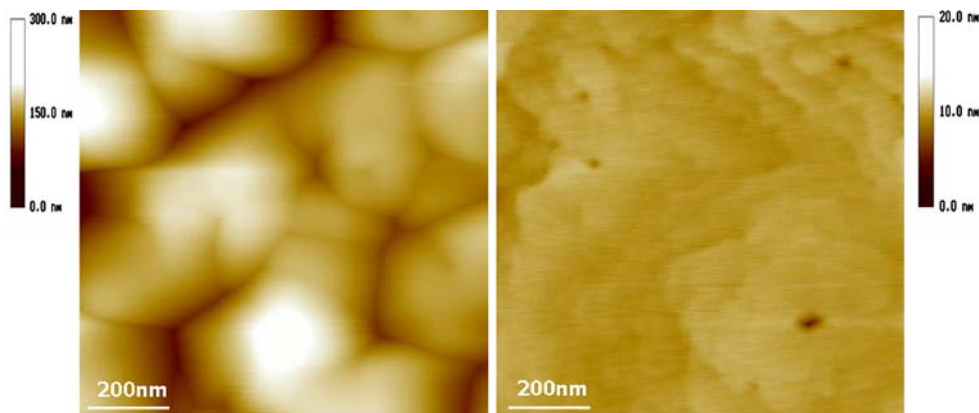


Fig. 2. AFM images: (a) ZnO epilayer on nitrided sapphire without MgO buffer layer and (b) ZnO epilayer on nitrided sapphire with MgO buffer layer.

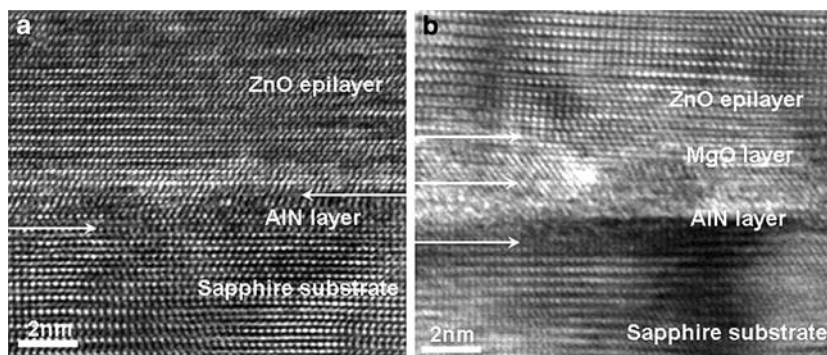


Fig. 3. HRTEM images along the $[10\bar{1}0]_{\text{sapph}}$ (a) without MgO buffer layer and (b) with MgO buffer layer.

AlN/Al₂O₃ interface region. A continuous cubic AlN layer of 2-nm thickness was formed with unrelaxed structure, indicating that it does not reduce the 18.3% lattice mismatch between ZnO and sapphire. An interface structure featured with misfit dislocations between AlN and ZnO was found, and more details are available in our work published elsewhere.¹⁶

Figure 3b shows the clear interfaces of ZnO/MgO/AlN/Al₂O₃. Above the unrelaxed zincblende AlN layer, displays a significant nonuniform MgO buffer with ~3-nm thickness. The MgO buffer can be resolved into two regions. One region can be distinguished as a 2-D wetting layer with about 1 nm located at the interface between MgO and AlN. The other region is a 3-D island layer with a regular rocksalt structure. The HRTEM micrograph agrees well with the S-K growth mode of MgO on the nitrided sapphire substrate, as observed in RHEED evolutions.

To explain the effect of the MgO buffer layer in the ZnO/nitrided sapphire (0001) heteroepitaxial system, we present a schematic diagram, as illustrated in Fig. 4. On the nitrided sapphire substrate, MgO is initially grown in the 2-D growth mode. Once it exceeds the critical thickness (about 1 nm), the misfit strain, caused by the 7.8% lattice mismatch between MgO and unrelaxed AlN, will be relaxed through the formation of islands. It is

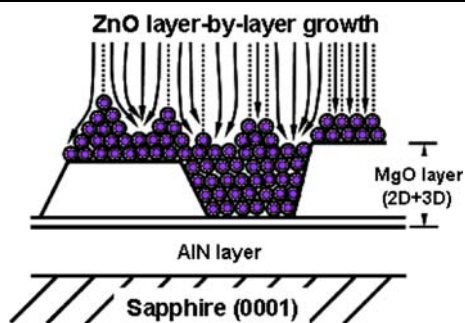


Fig. 4. Schematic diagram of the ZnO 2-D growth on the nucleated MgO thin layer.

noteworthy that the relaxation contributes to the lowering of the surface energy and reduction of the large mismatch. Another important effect of these islands is to provide nucleation sites for ZnO growth. They increase the wetting of a ZnO overlayer and promote the 2-D growth of the ZnO epilayer in the consequent deposition, finally resulting in a film with high quality and smooth surface. As reported before, the predominant dislocation in cubic MgO is not along the c -axis, but along the $\langle 110 \rangle$ direction.¹⁸ Thus, the interaction between dislocations might be introduced, which plays a key role in reducing TDs.¹⁹ We speculate that this may be another reason for the improved crystal quality. In the case of ZnO growth directly on nitrided sapphire, the lack of nucleation sites and the large lattice mismatch result in 3-D columnar growth and hence a rough surface and degraded quality.

In conclusion, a tri-buffer approach was applied to effectively reduce the large lattice mismatch between ZnO and nitrided sapphire, and a high-quality film with smooth surface was obtained. The effect of this method was systematically examined by RHEED, XRD, Raman spectroscopy, AFM, and TEM. A schematic diagram was proposed to understand the process. This method was found to be a viable way to obtain device-quality ZnO films.

ACKNOWLEDGEMENTS

This work is supported by the National Science Foundation (Grant Nos. 50532090, 60376004, and 60476044) and the Ministry of Science and Technology (Grant No. 2002CB613502) of China.

REFERENCES

1. X.-L. Guo, J.-H. Choi, H. Tabata, and T. Kawai, *Jpn. J. Appl. Phys.* 40, L177 (2001).
2. Y.R. Ryu, T.S. Lee, J.H. Leem, and H.W. White, *Appl. Phys. Lett.* 83, 4032 (2003).
3. H. Ohta, M. Orita, M. Hirano, and H. Hosono, *J. Appl. Phys.* 89, 5720 (2001).
4. H. Ohta, H. Mizoguchi, M. Hirano, S. Narushima, T. Kamiya, and H. Hosono, *Appl. Phys. Lett.* 82, 823 (2003).
5. H. Ohta, M. Hirano, K. Nakahara, H. Maruta, T. Tanabe, M. Kamiya, T. Kamiya, and H. Hosono, *Appl. Phys. Lett.* 82, 1029 (2003).

6. Y.I. Alivov, J.E. Van Nostrand, D.C. Look, M.V. Chukichev, and B.M. Ataev, *Appl. Phys. Lett.* 83, 2943 (2003).
7. Y.I. Alivov, D.C. Look, B.M. Ataev, M.V. Chukichev, V.V. Mamedov, V.I. Zinenko, Y.A. Agafonov, and A.N. Pustovit, *Solid-State Electron.* 48, 2343 (2004).
8. Y.I. Alivov, E.V. Kalinina, A.E. Cherenkov, D.C. Look, B.M. Ataev, A.K. Omaev, M.V. Chukichev, and D.M. Bagnall, *Appl. Phys. Lett.* 83, 4719 (2003).
9. K. Ip, Y.W. Heo, D.P. Norton, S.J. Pearton, J.R. LaRoche, and F. Ren, *Appl. Phys. Lett.* 85, 1169 (2004).
10. A. Tsukazaki, et al. , *Nat. Mater.* 4, 42 (2005).
11. Y. Ryu, T.-S. Lee, J.A. Lubguban, H.W. White, B.-J. Kim, Y.-S. Park, and C.-J. Youn, *Appl. Phys. Lett.* 88, 241108 (2006).
12. K. Iwata, P. Fons, S. Niki, A. Yamada, K. Matsubara, K. Nakahara, and H. Takasu, *Phys. Status Solidi A* 180, 287 (2000).
13. Y. Chen, H.-J. Ko, S.-K. Hong, and T. Yao, *Appl. Phys. Lett.* 76, 559 (2000).
14. H. Kato, K. Miyamoto, M. Sano, and T. Yao, *Appl. Phys. Lett.* 84, 4562 (2004).
15. M.W. Cho, A. Setiawan, H.-J. Ko, S.-K. Hong, and T. Yao, *Semicond. Sci. Technol.* 20, S13 (2005).
16. Z.X. Mei, Y. Wang, X.L. Du, M.J. Ying, Z.Q. Zeng, H. Zheng, J.F. Jia, Q.K. Xue, and Z. Zhang, *J. Appl. Phys.* 96, 7108 (2004).
17. Z.X. Mei, X.L. Du, Y. Wang, M.J. Ying, Z.Q. Zeng, H. Zheng, J.F. Jia, Q.K. Xue, and Z. Zhang, *Appl. Phys. Lett.* 86, 112111 (2005).
18. J.P. Hirth and J. Lothe *Theory of Dislocations* 2nd ed. Wiley, (New York, 1982).
19. Y. Chen, S.-K. Hong, H.-J. Ko, V. Kirshner, H. Wensch, T. Yao, K. Inaba, and Y. Segawa, *Appl. Phys. Lett.* 78, 3352 (2001).